One-step selective formation of silver nanoparticles on atomic layered MoS 2 by laser-induced defect engineering and photoreduction

Article *in* Journal of Materials Chemistry C · August 2017

DOI: 10.1039/C7TC01863K

CITATIONS
18

READS
712

6 authors, including:

Dawei Li
Dalian University of Technology
67 PUBLICATIONS **1,071** CITATIONS
SEE PROFILE

Tian Zhang
University of Nebraska at Lincoln
180 PUBLICATIONS **4,231** CITATIONS
SEE PROFILE

Xi Huang
University of Nebraska at Lincoln
62 PUBLICATIONS **1,123** CITATIONS
SEE PROFILE

Y. F. Lu
University of Nebraska at Lincoln
995 PUBLICATIONS **17,120** CITATIONS
SEE PROFILE

Journal of Materials Chemistry C

PAPER

Cite this: J. Mater. Chem. C, 2017, 5, 8883

One-step selective formation of silver nanoparticles on atomic layered MoS_2 by laser-induced defect engineering and photoreduction†

Y. T. Lei,[a] D. W. Li,*[b] T. C. Zhang,[a] X. Huang,[b] L. Liu[b] and Y. F. Lu[b]

Received 29th April 2017,
Accepted 3rd August 2017

DOI: 10.1039/c7tc01863k

rsc.li/materials-c

Two dimensional (2D) materials decorated with noble metal nanoparticles (NPs) have attracted wide attention due to their appealing chemical and physical properties. Herein, we have developed a novel approach to controllable and selective decoration of silver NPs on atomic layered molybdenum disulfide (MoS_2) by using one-step laser-induced defect engineering and photoreduction. By employing a focused micro-power laser beam, silver NPs can be rapidly (in seconds) anchored onto the irradiated area of MoS_2 flakes, forming 0D/2D AgNPs@MoS_2 heterostructures. The mechanism for silver growth on MoS_2 flakes was based on laser-induced defect creation in a silver ion environment and silver nucleation on laser-excited MoS_2 flake surfaces, as evidenced by a combination of techniques including Raman spectroscopy, atomic force microscopy and second-harmonic generation. We also found that the morphology and the growth rate of silver NPs are highly dependent on the layer thickness of MoS_2 and the laser irradiation power; while the size and number density of silver NPs could be precisely controlled by varying the irradiation time as well as the silver ion concentration. Finally, AgNPs@MoS_2 heterostructure micro-patterns have been successfully demonstrated *via* a programmed low-power laser scan, which shows great potential to be used as an efficient surface enhanced Raman scattering platform for chemical sensing.

Introduction

Recently, two dimensional (2D) semiconducting transition metal dichalcogenide (TMD) materials, such as molybdenum disulfide (MoS_2), have received tremendous attention due to their unique layer-dependent electrical and optical properties.[1–4] Bulk MoS_2 exhibits an indirect band gap of 1.29 eV, while monolayer MoS_2 has a direct band gap of ~1.90 eV with enhanced photoluminescence (PL).[5–8] Thus far, MoS_2 has achieved primary progress in the following fields: sensing,[9,10] energy harvesting,[11–13] and photoelectronic applications.[14,15] On the other hand, it is well known that noble metal nanoparticles (NPs) have broad applications in biosensing, catalysis, and photonics due to their excellent chemical and physical properties.[16–19] Therefore, fabrication of noble metal NPs with 2D TMDs, forming 0D/2D metal–semiconductor heterostructures, would promote the synergistic effect of both materials and expand their functionalities as novel catalytic, magnetic and optoelectronic materials.[20–23]

Among the potential applications of noble metal NP functionalized TMDs, surface enhanced Raman scattering (SERS) active substrates is one attractive area.[24–26] Traditionally, SERS substrates were made of noble metal NPs and low-concentration analytes were detected through the amplification of the electromagnetic field introduced by the surface plasma resonance effect.[27,28] Recently, 2D semiconductor materials, such as MoS_2, have been proved to have Raman enhancement effects due to their polar Mo–S bonds.[29] The low concentration of cytidine and adenosine molecules could be detected by few-layer MoS_2 due to a combination of the fluorescence quenching effect and modification of the local environment.[30] To date, several studies have been focused on the fabrication of noble metal NPs onto 2D MoS_2, forming 0D/2D NPs@MoS_2 heterostructures.[24–26,31–38]

In general, different methods have been explored for decorating noble metal NPs onto 2D materials, including physical deposition,[34,39,40] chemical reduction using different reducing agents,[31,36,37,41–44] light-induced reduction,[35,45–48] electrochemical method,[49,50] solvothermal method,[51,52] self-assembly method,[53,54] and wave-assisted reduction.[33,55,56] Among them, light-induced silver reduction on MoS_2 flakes represents a green and simple method as no additional chemical reagents need to

[a] Department of Civil Engineering, University of Nebraska-Lincoln, Omaha, NE 68182-0178, USA
[b] Department of Electrical and Computer Engineering, University of Nebraska-Lincoln, Lincoln, NE 68588-0511, USA. E-mail: dli8@unl.edu; Tel: +1 402-217-8863

† Electronic supplementary information (ESI) available: EDS spectrum, additional SEM images and silver ions concentration effect. See DOI: 10.1039/c7tc01863k

be added except silver nitrate itself, where MoS_2 acts as a photocatalyst and silver ions could be directly reduced and deposited on the photo-excited MoS_2 surfaces.[35] However, the growth rate of silver NPs on MoS_2 surfaces was slow *via* light exposure. In addition, selective and controlled decoration of silver NPs on MoS_2 surfaces could not be realized by the above method. Recently, a two-step approach for selective decoration of gold NPs on few-layer MoS_2 films has been reported, which is based on the self-assembly of Au NPs on premodified MoS_2 films with a focused laser beam.[26] However, a laser with a power greater than 20 mW is required for MoS_2 surface modification. Besides, the mechanism for the self-assembly process of Au on laser-modified MoS_2 surfaces was different from that of light-induced photo-reduction, since no laser was used during Au reduction. Considering the multi-step process and high-energy laser required in the above approach, it is promising to explore a simple, more efficient, cost-effective approach to realizing the selective and controllable decoration of noble metal NPs on 2D TMD surfaces. Meanwhile, an in-depth understanding of the noble metal NP growth mechanism on 2D materials is essential for practical applications.

In this work, we have developed a facile, one-step approach to selectively anchor silver NPs onto 2D MoS_2 sheets by a micro-power laser-induced defect engineering and photoreduction technique. The silver NP growth rate was fast, which could be realized in seconds with a micro-power laser in the presence of silver ion solution. We found that MoS_2 not only played the role of a photocatalyst but was also defected/consumed during the silver growth process, as evidenced by Raman spectroscopy, atomic force microscopy (AFM), and second harmonic generation (SHG). Based on these experimental results, we proposed a two-step silver growth mechanism on the MoS_2 surface using laser irradiation, which involves laser-induced surface defect creation in a silver ion solution and silver nucleation on laser excited MoS_2 surfaces. To the best of our knowledge, this is the first clear illustration of MoS_2 being defected/consumed during the silver growth process. Besides, the major parameters impacting the size, shape, and number density of the deposited silver NPs were identified and evaluated. Moreover, the as-prepared 0D/2D AgNPs@MoS_2 heterostructures were free of any capping agents and exhibited good SERS activity, showing great potential for chemical sensing application. Our work thus provides a new avenue for selectively functionalizing MoS_2 with noble metal NPs in a simple, rapid, green and cost-effective way.

Materials and methods

Reagents and materials

Silver nitrate (purity > 99%), gold(III) chloride trihydrate (>99.9% trace metal basis) and Rhodamine 6G (R6G) (R4127, ~95%) were purchased from Sigma-Aldrich (St. Louis, MO, USA) and used without further purification. SiO_2/Si wafers (285 nm, PC lot # O-9086, SQI, San Jose, CA, USA) were cut into 6 mm × 8 mm substrates and used for MoS_2 flake transfer. High purity grade methanol purchased from Fisher Scientific (Fair Lawn, NJ, USA) was used as a solvent for R6G solution preparation. Deionized water (electrical resistivity = 18 MΩ cm) used for silver nitrate solution preparation and washing was made with the Millipore Simplicity System (Thermo Fisher Scientific Inc., US). The mechanically exfoliated MoS_2 was chosen to get high-quality MoS_2 flakes with fewer defects. MoS_2 flakes were obtained by microcleavage of natural bulk crystals (Graphene Supermarket) using Scotch® transparent tape.

Experimental design

Silver NP decorated MoS_2 composites were first synthesized by immersing the exfoliated multiple layered (M L) MoS_2 substrates in silver nitrate solution (1 mM) and irradiated with a focused laser beam (633 nm, 25 μW) for a certain time (*e.g.*, 7 s) using a 50× objective. The spot size for a 633 nm laser focused onto the sample is ~1.5 μm. After laser irradiation, the substrates were taken out and washed in deionized water. At the same time, a control experiment was conducted under the same conditions except that no external laser source or MoS_2 flakes were provided. In order to investigate the mechanism of laser-induced silver growth on the MoS_2 surfaces, lasers with different wavelengths (514.5, 633, and 785 nm) were tested for silver NP growth. To realize the controllable preparation of silver NPs by size, shape and number density, the impact of process parameters, including MoS_2 layer numbers, laser power, irradiation time and silver nitrate concentration, was systemically investigated in different tests. Unless mentioned elsewhere or investigated, the monolayer (1 L) MoS_2 flake, 1 mM $AgNO_3$, 633 nm laser with a power of 25 μW and the irradiation time of 7 s were kept constant for the AgNPs@MoS_2 heterostructure fabrication.

Characterization methods

1 L, bilayer (2 L), and few-layer (F L) MoS_2 flakes were exfoliated onto a SiO_2/Si substrate and identified by optical microscopy (Nikon ECLIPSE LV150) and Raman spectroscopy. Both Raman and PL measurements were performed at room temperature in the same micro-Raman system (Renishaw inVia 2000). The Raman scattering was excited by a 514 nm Ar^+ laser with a power of ~200 μW, while the PL scattering was excited by a 633 nm laser with a power of ~20 μW to avoid heating. Morphological characterization of AgNPs@MoS_2 was carried out through a field emission scanning electron microscope (SEM, JEOL JSM-7600F). An AFM (Bruker Multimode 8 AFM) operated in the peak-force working mode was applied to study the morphological evolution of laser-irradiated 2D MoS_2. SHG imaging measurement was conducted using a multiphoton nonlinear optical microscopy system according to our previous reports.[4,57] The size and density distribution of silver NPs formed was analysed by MATLAB (2016a).

SERS study

The SERS activity of the as-fabricated AgNPs@MoS_2 heterostructures was investigated, wherein R6G was chosen as the probe molecule in the SERS study. 100 μL of 1 μM R6G solution (dissolved in methanol) was dropped onto the as-fabricated SERS substrates and dried in air at room temperature.

Raman spectra of R6G were recorded with the micro-Raman system using a 50× objective with a numerical aperture of 0.75. The excitation source was a focused 633 nm laser with a power of 0.5 to 1 mW. For comparison, Raman scattering from the bare SiO_2/Si substrate and MoS_2 flakes without laser irradiation was also collected.

Results and discussion

Formation mechanism of AgNPs@MoS_2 heterostructures

In this work, silver NPs were found to be rapidly and selectively formed on the exfoliated layered MoS_2 surfaces in the presence of silver ions upon focused laser beam irradiation. As shown in Fig. 1a, a significant optical contrast change was obtained for the arrowed MoS_2 after focused laser irradiation (633 nm, 25 μW) for 7 s in silver nitrate solution. Both the SEM image (Fig. 1b) and the energy dispersive X-ray spectrum (Fig. S1, ESI†) indicated that silver NPs were formed in the laser irradiated region. Similarly, gold NPs could be formed on the MoS_2 surface through the same route if we substitute the silver nitrate with gold chloride (Fig. S2, ESI†), suggesting the universality of the laser irradiation method in the synthesis of noble metal NPs on the surface of atomic layered TMDs.

Control experiments without MoS_2 flakes or laser irradiation have been conducted to further understand the mechanism of the reaction. In both cases, no significant change in colour was observed through optical imaging, indicating no growth of silver NPs (data not shown). This means that both MoS_2 flakes and focused laser beam irradiation have played important roles

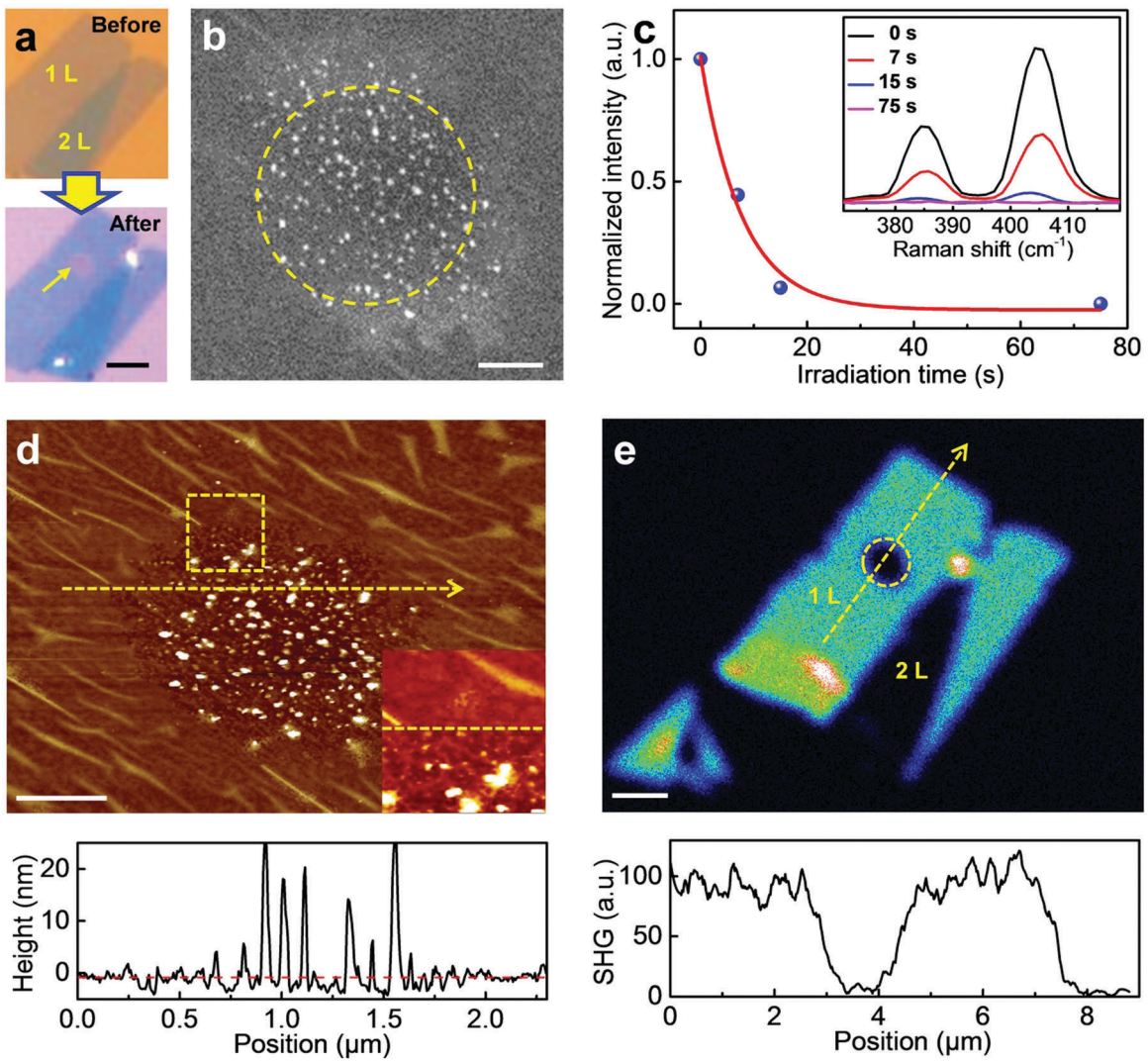

Fig. 1 (a) Optical images of 1 L MoS_2 flake immersed in 1 mM $AgNO_3$ solution before and after irradiation with a focused 633 nm laser (25 μW) for 7 s. The yellow arrowed position is the laser focus spot. (b) Enlarged SEM image of the irradiated MoS_2 in the laser focus spot. (c) Normalized Raman intensity of A_{1g} peak of 1 L MoS_2 after 633 nm laser irradiation (25 μW) in $AgNO_3$ solution as a function of laser irradiation time. Inset shows the corresponding Raman spectra. (d) AFM topography image of laser irradiated spot on 1 L MoS_2. Inset is the enlarged yellow dashed square area in (d). The cross-sectional height profile along the yellow dashed line shows that the average silver NP size is around 20 nm. (e) SHG image and cross-sectional intensity profile of the same sample in (a) after laser irradiation. Scale bars: 5 μm in (a), 500 nm in (b and d) and 2 μm in (e).

in silver growth. More interestingly, we found that MoS_2 was defected/consumed during the silver growth process (Fig. 1). This observation is different from the previously reported light-driven growth of silver NPs on 2D MoS_2, where MoS_2 only played the role of photocatalyst for the silver reduction.[35] To check the role MoS_2 played during the silver growth process in our work, the evolution of Raman spectra for the 1 L MoS_2 sheet immersed in a silver nitrate solution and irradiated with a 633 nm laser for different times was recorded (Fig. 1c). Compared with MoS_2 flakes without laser irradiation, a decrease of the peak intensity of A_{1g} was observed for MoS_2 irradiated with laser for 7 s. With further increasing laser irradiation time, the Raman peak intensity of MoS_2 decreased exponentially and almost disappeared when the irradiation time reached 75 s. This revealed that the MoS_2 sheet was defected and consumed during the silver growth process.

AFM and SHG measurements were taken to further prove MoS_2 was defected during the silver growth. As shown in Fig. 1d, silver NPs with a size of ~20 nm as well as defects (Fig. 1d inset) were clearly observed on the laser irradiated MoS_2 surface. SHG imaging is an effective tool for rapid evaluation of the crystal quality of 1 L MoS_2.[4] One can see that the SHG intensity for 1 L MoS_2 vanished at the laser focus spot (Fig. 1e), revealing that the atomic structure of MoS_2 was damaged after micro-power laser irradiation in silver ion solution. However the laser power we employed was very low, ~25 μW, which was much weaker and not high enough to cause thermal defects on MoS_2.[26] Thus, we proposed that the defects on MoS_2 surface were created as a result of both laser excitation and the presence of silver ions. This indicated that the mechanism of silver growth on MoS_2 *via* laser irradiation was different from the previous report.[35]

The effect of the surface defects of MoS_2 on silver growth was further investigated by laser irradiation with ultralow power (Fig. 2). Herein, two different MoS_2 spots, one in the centre and the other one on the edge, were both irradiated by a 633 nm laser with a power as low as ~0.05 μW for 20 min (Fig. 2a). Small and low-density silver NPs as well as defects were observed at the edge of the MoS_2 sheet (Fig. 2b). In contrast, neither defects nor silver NPs were observed in the irradiated spot in the centre after 0.05 μW laser irradiation for the same length of time (Fig. 2c). It is observed that the edge of MoS_2 shows more defects than the centre, which easily creates more surface defects (or active sites) during the silver growth upon laser irradiation, as was evidenced by Raman spectra recorded for the irradiated spot on the edge (Fig. 2d) where the peak intensity decreased and the peak distance between A_{1g} and E^1_{2g} broadened. Thus, surface defects played an important role for laser-induced silver nucleation and growth on 2D MoS_2 surfaces.

Based on the above experimental results, we proposed a two-step silver growth mechanism on the MoS_2 surface by laser irradiation in silver ion solution (Fig. 2e). Upon laser irradiation with an appropriate wavelength, 2D semiconducting MoS_2 sheets will be photo-excited, generating electron hole pairs.

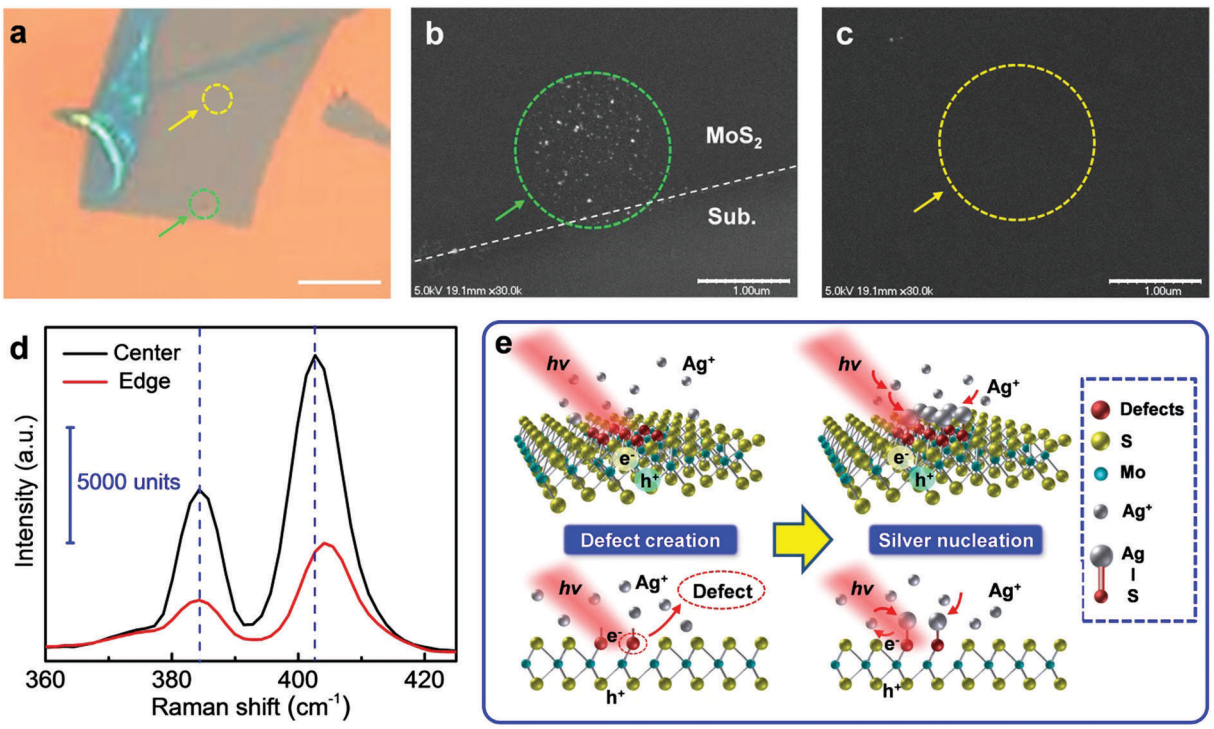

Fig. 2 (a) Optical image of 1 L MoS_2 after focused 633 nm laser irradiation (0.05 μW) for 20 min in 1 mM $AgNO_3$ solution. The two dash circled areas represent the laser focus spots. Enlarged SEM images of the (b) green and (c) yellow dash circled areas in (a). (d) Raman spectra of two points on 1 L MoS_2 in (a). (e) Schematic illustration of laser-induced formation of silver NPs on 2D MoS_2 nanosheets. Scale bars: 5 μm in (a) and 1 μm in (b and c).

With the presence of silver ions, surface defects in the form of unbound sulfur are expected to be created on the laser-excited MoS_2 surface if the laser power is appropriate (micro-power). Then, the laser-induced unbound S bonds on the defect sites of MoS_2 can reduce silver ions and act as the bonding sites for silver nucleation,[26] leading to the deposition of silver on the MoS_2 surface defects under photoexcitation. The one-step process of laser-induced defect creation and silver growth could be realized in seconds (within 7 s) with low laser power ($\sim$25 μW), suggesting its potential for low-cost, large-scale fabrication of silver NPs on 2D MoS_2.

The effect of laser wavelength on silver growth on 1 L MoS_2 surfaces was also investigated (Fig. 3). Fig. 3a–c compare the PL spectra of 1 L MoS_2 collected with three different excitation laser wavelengths. The 785 nm laser has a photon energy of 1.58 eV, which is not high enough to excite 1 L MoS_2 ($\sim$1.9 eV). It was expected that no significant PL signal could be obtained using the 785 nm laser, which was consistent with the PL measurement (Fig. 3c). Accordingly, no silver growth was observed under the irradiation of the 785 nm laser even with a high power of $\sim$25 mW (Fig. 3f and i). For irradiation lasers with shorter wavelengths, such as 633 and 514 nm, their photon energies exceed the bandgap of 1 L MoS_2, as evidenced by the PL spectral measurement (Fig. 3a and b). Thus, the growth of silver NPs was realized with 633 and 514 nm laser irradiation (Fig. 3d and e). Fig. 3g–i compare the SEM images of silver NPs formed under the irradiation of 633 and 514 nm lasers. The focus laser spot sizes were $\sim$1 μm and $\sim$1.5 μm for the 514 and 633 nm lasers, respectively. However, the growth area of silver NPs formed by the 514 nm laser was bigger than that of the 633 nm, as evidently revealed by the SEM images (Fig. 3g and h). This was attributed to more silver ions reduced by the higher photon energy of the laser with a shorter wavelength. These results further prove that defect creation and silver NP growth are based on the laser excitation of MoS_2.

Besides, several silver NPs were randomly formed at the edges or other spots, other than the laser irradiated spot (Fig. S3, ESI†). This can be rationalized by the presence of room light during the laser focus process and the rapid reduction of silver ions at the surface defects during the preparation process.[35,58]

Silver NP growth rate and morphological control

SEM images shown in Fig. 4a–c reveal that the growth rate and the morphologies of silver NPs were highly layer number dependent. With the same process parameters, a focused laser beam led to the formation of silver NPs with a growth area of 2 μm and a uniform size of $\sim$20 nm (Fig. 4a). In contrast, we observed that bigger silver NPs with a size of around 40 nm

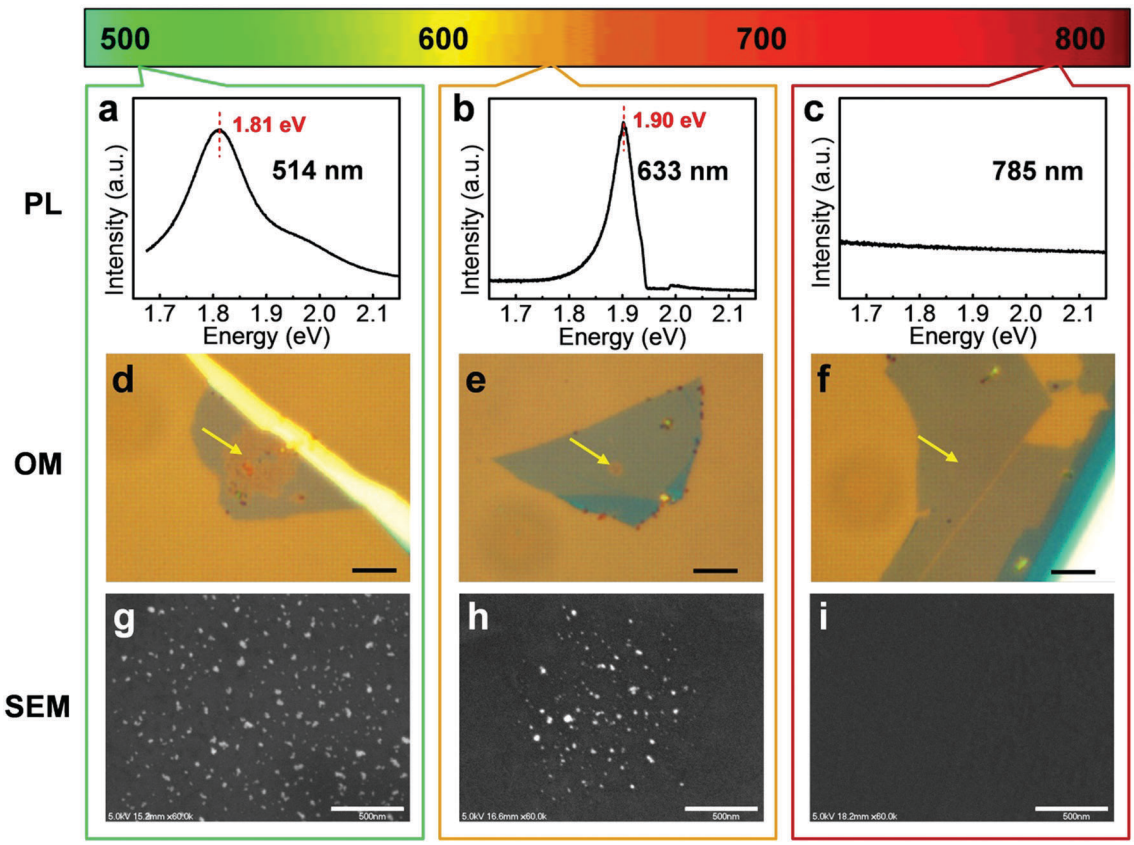

Fig. 3 Laser wavelength effect. PL spectra of 1 L MoS_2 sheets by excitation laser with wavelengths of (a) 514 nm, (b) 633 nm and (c) 785 nm. (d–f) Optical and (g–i) SEM images of silver NPs formed on 1 L MoS_2 in 1 mM $AgNO_3$ solution after irradiation *via* laser with a wavelength of (d and g) 514 nm, (e and h) 633 nm and (f and i) 785 nm for 7 s. The yellow arrowed positions in (d–f) point to the laser irradiation spots. Scale bars: 5 μm in (d–f) and 500 nm in (g–i).

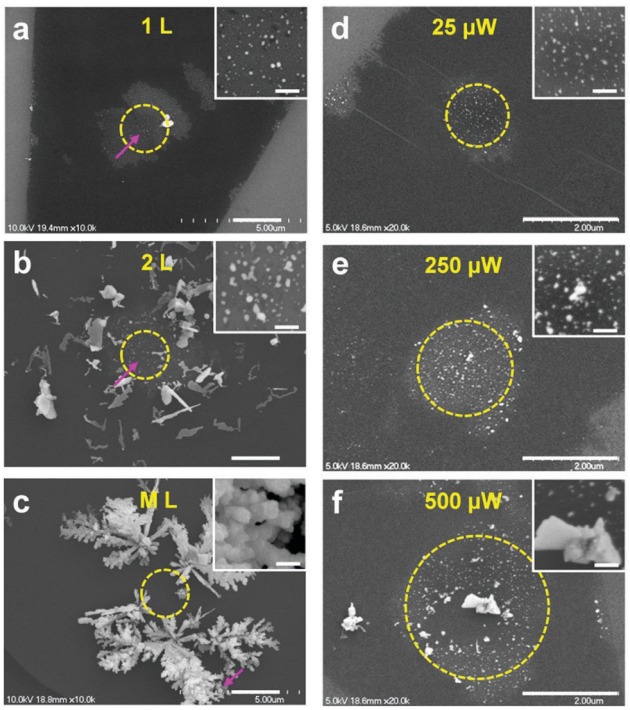

Fig. 4 SEM images of the AgNPs@MoS_2 heterostructures grown in 3 mM $AgNO_3$ on (a) 1 L, (b) 2 L and (c) M L MoS_2 with 633 nm laser (250 μW) irradiation for 7 s. The yellow circled positions in (a–c) point to the laser irradiation spots. The insets show high magnification images of the purple arrowed areas. SEM images of the AgNPs@MoS_2 heterostructures grown in 1 mM $AgNO_3$ on 1 L MoS_2 under laser powers of (d) 25, (e) 250 and (f) 500 μW for 7 s. The insets show high magnification images of the yellow centered areas. Scale bars: 2 μm in (a–f) and 500 in insets of (a–f).

were formed on 2 L MoS_2 in the laser focus spot, meanwhile big silver flakes/platelets of up to 1 μm were developed on the perimeters of the focus centre (Fig. 4b). When the M L MoS_2 flake was illuminated, silver dendrites of up to several micrometres were developed on the laser focused area (Fig. 4c), indicating a faster silver NP growth rate on thick MoS_2 layers. The high magnification SEM image (inset in Fig. 4c) shows that each branch was composed of silver NPs with a size of around 500 nm.

The faster growth rate of silver NPs on 2 L and M L MoS_2 than that on the 1 L MoS_2 surface could be explained by the transition from an indirect to a direct semiconductor. As we know, the electrons used for silver reduction were provided by laser-excited MoS_2. Compared to M L and 2 L MoS_2, 1 L MoS_2 has a decreased amount of freely mobile photo-generated electrons due to the increased exciton binding energy and reduced lifetime of the charged carriers.[59] Besides, M L MoS_2 absorbed more photon energies than the few-layer/1 L MoS_2.[60] Therefore, more defects were created on M L MoS_2 due to more photo-generated electrons, leading to much faster nucleation and crystallization of silver on M L MoS_2 compared with 1 L MoS_2.

Similar control of the growth rate and morphology of silver NPs was also achieved by tuning the laser power intensity. In our experiment, no silver NPs were observed on the irradiated spots when the laser power was 0.05 μW even with a long irradiation time of 20 minutes in silver ion solution (Fig. 2), which was attributed to no defects being created on the 1 L MoS_2 surface with such a low laser power. When the laser power was increased to 25 μW, significant silver NP growth was observed with a short irradiation time of 7 s (Fig. 4d). This reveals that there is a threshold (micro-power) for the defect creation and silver nucleation on MoS_2 by laser in the presence of silver ions. As shown in Fig. 4d–f, by increasing laser power from 25 to 500 μW, the diameter of the silver NP growth area was expanded from 1 to 3 μm. This is due to the bigger impact area introduced by the laser with a higher power intensity. It has been reported that higher power would promote the nucleation and growth of silver NPs due to the elevated reduction power of the reaction system provided.[61] As revealed in Fig. 4d and e, uniformly distributed silver NPs with a size around 20–30 nm were observed for a laser power within 250 μW, while bigger silver crystals with a size up to 1 μm were formed when the laser power increased to 500 μW (Fig. 4f), indicating that the growth rate of silver NPs was impacted by laser power. Much bigger aggregates were formed when the laser power was 25 mW (Fig. S4, ESI†). It is interesting to note that fewer and less dense silver NPs were observed around the bigger silver aggregates. This was considered to be due to the Ostwald ripening, which means the growth of big aggregates will sacrifice the surrounding small NPs.[62] Thus, to get denser and more uniformly distributed silver NPs, a smaller laser power between 25 and 250 μW should be chosen to avoid big aggregate formation.

To investigate the effect of temperature increase of the MoS_2 sheet by laser irradiation during silver growth, the temperature change in 1 L and M L MoS_2 was measured *via* the shifts in the Raman peak of the E^1_{2g} band (Fig. S5 and S6, ESI†).[63,64] We estimated the temperature change in MoS_2 using eqn (1) as follows:

$$\Delta T = \frac{\chi_P}{\chi_T} P, \quad (1)$$

where χ_P, χ_T and P represent the fitted linear power coefficient, the fitted linear temperature coefficient, and the laser power, respectively. The temperature increase for 1 L MoS_2 was calculated to be ~18.5 K during laser irradiation with a power of 25 mW (Fig. S5, ESI†). A similar estimation revealed that the temperature increase for M L MoS_2 was a little higher, around 41 K, with the same laser power. This temperature increase was much lower than the temperature required for thermolysis of silver nitrate.[65] Plus, the laser power we employed for fabricating AgNPs@MoS_2 heterostructures was within 250 μW, of which the corresponding temperature increase was less than 1 K. Thus, the effect of temperature increase in our experiment can be neglected.

Silver NP size and number density control

The effects of laser irradiation time, silver ion concentration on NP size and number density were investigated. As revealed in Fig. 5a, with a short exposure time (~3 s), the 1 L MoS_2 flake

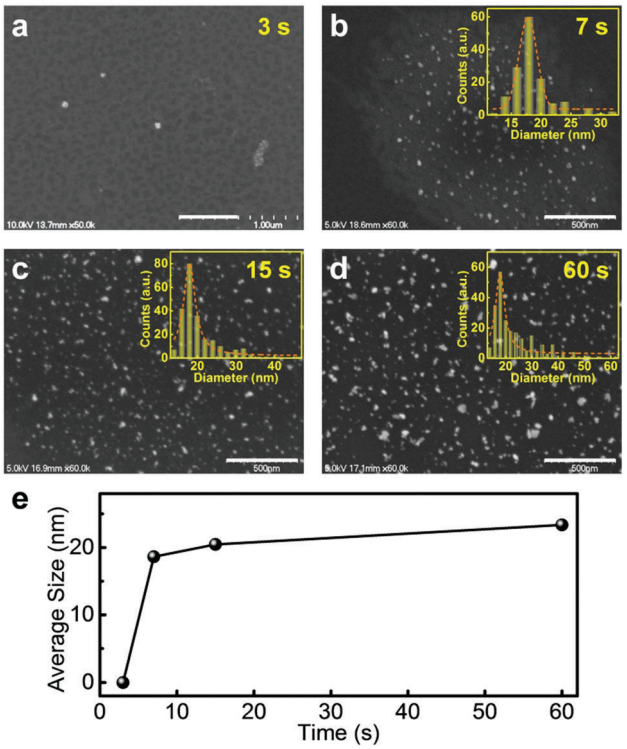

Fig. 5 Laser irradiation time impact. SEM images of the AgNPs@MoS_2 heterostructures grown in 1 mM $AgNO_3$ on 1 L MoS_2 with 633 nm laser irradiation (25 μW) for (a) 3 s, (b) 7 s, (c) 15 s and (d) 60 s. Scale bars: 500 nm. The insets show the corresponding size distribution of silver NPs formed under different irradiation times. (e) The average size of silver NPs as a function of laser irradiation time.

was "etched" into smaller nanosheets, leading to the formation of more defect sites in the laser irradiated region, which is consistent with our proposed laser-induced defect engineering mechanism (Fig. 2e). When the exposure time increased to 7 s, more and denser silver NPs formed on these defect sites (Fig. 5b). Moreover, with a longer irradiation time (~60 s), the silver NPs grew bigger and began to aggregate. The histograms in the insets of Fig. 5b–d summarize the corresponding size distribution of the silver NPs. The size distribution of silver NPs formed after 7 s laser irradiation complies with the Gaussian profile with the peak position centering at around 18 nm, which is in good agreement with AFM measurement (Fig. 1d). As the laser irradiation time increased, more silver NPs were formed and silver NPs with a bigger size emerged. Fig. 5e shows the average silver NP size as a function of laser irradiation time. We could see that the average size of silver NPs grew from 18 to 23 nm with irradiation increasing from 7 to 60 s. This indicates that the size of silver NPs could be well controlled by tuning the laser irradiation time.

A similar impact on the size and number density of silver NPs was observed by tuning the silver ion concentration (Fig. S7, ESI†). We could see that increasing of $AgNO_3$ concentration from 0.3 to 3 mM led to more and denser silver NPs deposited onto the MoS_2 surfaces. Big silver NPs aggregating from small silver NPs were evidently shown on MoS_2 hybrids made with 10 mM $AgNO_3$. The formation of these bigger NPs scarified the surrounding small NPs and thus decreased the density of silver NPs deposited on the MoS_2 surface, which could be explained using the Ostwald ripening growth mechanism.[62]

SERS study

Finally, we demonstrated the selective decoration of silver NPs on the exfoliated MoS_2 flakes, forming patterned 0D/2D AgNPs@MoS_2 heterostructures. Meanwhile, their SERS activities were investigated. As shown in Fig. 6a, an area of black dots formed at each focused laser irradiated spot. SEM images (Fig. S8, ESI†) revealed that each black dot was a group of silver NPs with a size of around 500 nm. A patterned AgNPs@MoS_2 array was obtained in the MoS_2 flakes immersed in silver nitrate solution by using a scanning laser with a programmed pattern. These results show that silver NPs could be rapidly and selectively formed in a controllable manner on the MoS_2 surface by one-step laser irradiation in silver ion solution.

Fig. 6b shows the Raman mapping plotted for the Raman signals measured at 1507 cm^{-1} for R6G on the AgNPs@MoS_2 patterned array. We can see that the Raman mapping corresponds well to the shape of the investigated pattern array, which reveals that the Raman enhancement mainly originated from the silver NPs formed on MoS_2 flakes. To further prove this, the Raman spectra of R6G on AgNPs@MoS_2 and the MoS_2 flake without laser irradiation were compared (Fig. 6c). No vibration mode of R6G was observed on the MoS_2 flakes itself. In contrast, Raman signals with distinct peaks, high intensity and a strong signal-to-noise ratio were observed on the AgNPs@MoS_2 region. A simple analytical factor, which was defined as $(I_{SERS}/I_{ref})/(C_{SERS}/C_{ref})$, was used to calculate the SERS enhancement factor (EF), where C_{ref} and C_{SERS} represent the concentrations of R6G used for obtaining the I_{ref} and I_{SERS}, respectively, in measurements.[66,67] Herein, we chose the Raman spectra of R6G on bare SiO_2/Si substrates with subtracted background as references. The concentrations of R6G used for SERS and normal reference Raman spectra measurement are 1 μM and 100 mM, respectively (Fig. S9, ESI†). I_{ref} and I_{SERS} measured at 1507 cm^{-1} for R6G are 1.74×10^4 and 576, respectively. Therefore, the EF was calculated to be $\sim 3 \times 10^6$, indicating a good SERS performance for the as-fabricated AgNPs@MoS_2 heterostructures which can be further improved by optimizing AgNPs@MoS_2 growth parameters.

Fig. 6d shows the Raman line mapping of R6G measured along the green dashed lined area in Fig. 6b. A periodic change of the Raman intensity measured at 1507 cm^{-1} was revealed, which further proved that the Raman enhancement was due to the silver NPs selectively formed on the MoS_2 surfaces. Furthermore, it is clearly seen that the AgNPs@MoS_2 heterostructure has uniform Raman enhancement. The standard deviation was calculated to be within 20%, which proves the uniformity of the fabricated 0D/2D heterostructures and thus they could be used as efficient and uniform SERS-active substrates. Moreover, the stability of the as-fabricated AgNPs@MoS_2 heterostructures was examined by immersing the substrates into deionized water for a week (Fig. S10, ESI†). No obvious change in morphology was

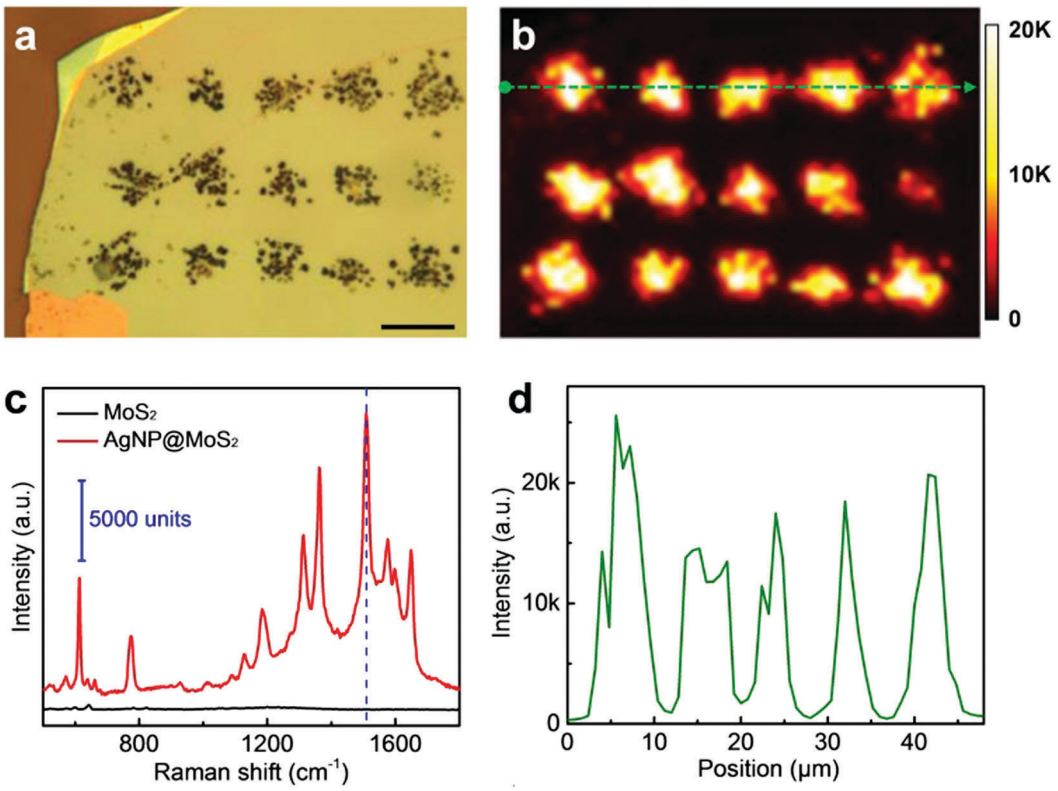

Fig. 6 (a) Optical image of patterned AgNPs@MoS_2 heterostructures formed on a multiple layer MoS_2 flake by a programmed 633 nm laser scan. Scale bar: 10 μm. (b) Raman mapping of R6G at 1507 cm^{-1} measured on patterned AgNPs@MoS_2 heterostructures. (c) Raman spectra of R6G (1 μM) absorbed onto the AgNPs@MoS_2 heterostructure (red) and MoS_2 flake without laser scan (black). (d) The Raman peak intensity measured at 1507 cm^{-1} of the hybrid structures marked by the green dashed line in (b).

observed, indicating the stable structure of AgNPs@MoS_2, namely, good interaction between silver NPs and MoS_2 surfaces.

Conclusions

We have developed a facile, rapid and one-step approach to selective decoration of silver NPs on atomic layered MoS_2 *via* micro-power focused laser irradiation treatment. The mechanism for laser-induced growth of silver NPs was based on the creation of surface defects together with photocatalytic reduction on the laser-excited MoS_2 surface. The reaction could be realized within seconds and with low laser power within several microwatts. Silver NPs could be selectively formed on the MoS_2 surfaces with programmed laser irradiation. The study on the impact parameters showed that the size, number density, and growth rate of the silver NPs formed could be tuned. The as-fabricated 0D/2D AgNPs@MoS_2 heterostructures also exhibited an efficient and uniform SERS effect with a standard deviation of less than 20%.

Acknowledgements

This research was financially supported by the Chinese Scholarship Council (CSC), the National Science Foundation (CMMI 1068510, CMMI 1129613, CMMI 1265122), and the University of Nebraska-Lincoln.

Notes and references

1 B. Radisavljevic, A. Radenovic, J. Brivio, I. V. Giacometti and A. Kis, *Nat. Nanotechnol.*, 2011, **6**, 147–150.
2 Y. Li, H. Wang, L. Xie, Y. Liang, G. Hong and H. Dai, *J. Am. Chem. Soc.*, 2011, **133**, 7296–7299.
3 Z. Yin, H. Li, H. Li, L. Jiang, Y. Shi, Y. Sun, G. Lu, Q. Zhang, X. Chen and H. Zhang, *ACS Nano*, 2012, **6**, 74–80.
4 D. Li, W. Xiong, L. Jiang, Z. Xiao, H. Rabiee Golgir, M. Wang, X. Huang, Y. Zhou, Z. Lin and J. Song, *ACS Nano*, 2016, **10**, 3766–3775.
5 D. Li, Z. Xiao, H. R. Golgir, L. Jiang, V. R. Singh, K. Keramatnejad, K. E. Smith, X. Hong, L. Jiang and J. F. Silvain, *Adv. Electron. Mater.*, 2017, **3**, 1600335.
6 K. F. Mak, C. Lee, J. Hone, J. Shan and T. F. Heinz, *Phys. Rev. Lett.*, 2010, **105**, 136805.
7 A. Splendiani, L. Sun, Y. Zhang, T. Li, J. Kim, C.-Y. Chim, G. Galli and F. Wang, *Nano Lett.*, 2010, **10**, 1271–1275.
8 D. Li, Q. Zou, H. Rabiee-Golgir, K. Keramatnejad, X. Huang, J. Song, Z. Xiao, L. Fan, X. Hong and L. Jiang, *Nanoscale*, 2017, **9**, 8997–9008.
9 H. Li, Z. Yin, Q. He, H. Li, X. Huang, G. Lu, D. W. H. Fam, A. I. Y. Tok, Q. Zhang and H. Zhang, *Small*, 2012, **8**, 63–67.
10 D. Jariwala, V. K. Sangwan, L. J. Lauhon, T. J. Marks and M. C. Hersam, *ACS Nano*, 2014, **8**, 1102–1120.

11 S. Ding, D. Zhang, J. S. Chen and X. W. D. Lou, *Nanoscale*, 2012, **4**, 95–98.
12 B. Hinnemann, P. G. Moses, J. Bonde, K. P. Jørgensen, J. H. Nielsen, S. Horch, I. Chorkendorff and J. K. Nørskov, *J. Am. Chem. Soc.*, 2005, **127**, 5308–5309.
13 M. A. Lukowski, A. S. Daniel, F. Meng, A. Forticaux, L. Li and S. Jin, *J. Am. Chem. Soc.*, 2013, **135**, 10274–10277.
14 M. Buscema, M. Barkelid, V. Zwiller, H. S. van der Zant, G. A. Steele and A. Castellanos-Gomez, *Nano Lett.*, 2013, **13**, 358–363.
15 H. S. Lee, S.-W. Min, Y.-G. Chang, M. K. Park, T. Nam, H. Kim, J. H. Kim, S. Ryu and S. Im, *Nano Lett.*, 2012, **12**, 3695–3700.
16 P. K. Jain, X. Huang, I. H. El-Sayed and M. A. El-Sayed, *Plasmonics*, 2007, **2**, 107–118.
17 T. K. Sau, A. L. Rogach, F. Jäckel, T. A. Klar and J. Feldmann, *Adv. Mater.*, 2010, **22**, 1805–1825.
18 G. Doria, J. Conde, B. Veigas, L. Giestas, C. Almeida, M. Assunção, J. Rosa and P. V. Baptista, *Sensors*, 2012, **12**, 1657–1687.
19 P. K. Jain, X. Huang, I. H. El-Sayed and M. A. El-Sayed, *Acc. Chem. Res.*, 2008, **41**, 1578–1586.
20 S. Su, H. Sun, F. Xu, L. Yuwen and L. Wang, *Electroanalysis*, 2013, **25**, 2523–2529.
21 P. Zhang, X. Lu, Y. Huang, J. Deng, L. Zhang, F. Ding, Z. Su, G. Wei and O. G. Schmidt, *J. Mater. Chem. A*, 2015, **3**, 14562–14566.
22 Z. Yin, B. Chen, M. Bosman, X. Cao, J. Chen, B. Zheng and H. Zhang, *Small*, 2014, **10**, 3537–3543.
23 J. Kim, S. Byun, A. J. Smith, J. Yu and J. Huang, *J. Phys. Chem. Lett.*, 2013, **4**, 1227–1232.
24 J. Zhao, Z. Zhang, S. Yang, H. Zheng and Y. Li, *J. Alloys Compd.*, 2013, **559**, 87–91.
25 S. Su, C. Zhang, L. Yuwen, J. Chao, X. Zuo, X. Liu, C. Song, C. Fan and L. Wang, *ACS Appl. Mater. Interfaces*, 2014, **6**, 18735–18741.
26 J. Lu, J. H. Lu, H. Liu, B. Liu, L. Gong, E. S. Tok, K. P. Loh and C. H. Sow, *Small*, 2015, **11**, 1792–1800.
27 P. L. Stiles, J. A. Dieringer, N. C. Shah and R. P. Van Duyne, *Annu. Rev. Anal. Chem.*, 2008, **1**, 601–626.
28 D. Li, S. Wu, Q. Wang, Y. Wu, W. Peng and L. Pan, *J. Phys. Chem. C*, 2012, **116**, 12283–12294.
29 L. Sun, H. Hu, D. Zhan, J. Yan, L. Liu, J. S. Teguh, E. K. Yeow, P. S. Lee and Z. Shen, *Small*, 2014, **10**, 1090–1095.
30 H. Qiu, Z. Li, S. Gao, P. Chen, C. Zhang, S. Jiang, S. Xu, C. Yang and H. Li, *RSC Adv.*, 2015, **5**, 83899–83905.
31 Z. Wu, L. Xie, Y. Xiao and D. Wang, *J. Alloys Compd.*, 2017, **708**, 763–768.
32 A. Lavie, L. Yadgarov, L. Houben, R. Popovitz-Biro, T.-E. Shaul, A. Nagler, H. Suchowski and R. Tenne, *Nanotechnology*, 2017, **28**, 24LT03.
33 X. Li, J. Zhu and B. Wei, *Chem. Soc. Rev.*, 2016, **45**, 3145–3187.
34 A. M. Yan, Y. Hua and V. P. Dravid, *Appl. Phys. Lett.*, 2016, **108**, 091901.
35 T. Daeneke, B. Carey, A. Chrimes, J. Z. Ou, D. Lau, B. Gibson, M. Bhaskaran and K. Kalantar-Zadeh, *J. Mater. Chem. C*, 2015, **3**, 4771–4778.
36 Z. Cheng, B. He and L. Zhou, *J. Mater. Chem. A*, 2015, **3**, 1042–1048.
37 L. Zhou, B. He, Y. Yang and Y. He, *RSC Adv.*, 2014, **4**, 32570–32578.
38 P. Zuo, L. Jiang, X. Li, B. Li, Y. Xu, X. Shi, P. Ran, T. Ma, D. Li and L. Qu, *ACS Appl. Mater. Interfaces*, 2017, **9**, 7447–7455.
39 S. U. Yu, B. Park, Y. Cho, S. Hyun, J. K. Kim and K. S. Kim, *ACS Nano*, 2014, **8**, 8662–8668.
40 Z. Luo, L. A. Somers, Y. Dan, T. Ly, N. J. Kybert, E. Mele and A. Johnson, *Nano Lett.*, 2010, **10**, 777–781.
41 X.-Z. Tang, Z. Cao, H.-B. Zhang, J. Liu and Z.-Z. Yu, *Chem. Commun.*, 2011, **47**, 3084–3086.
42 P. Xu, H. Yu and X. Li, *Chem. Commun.*, 2012, **48**, 10784–10786.
43 C. Xu, X. Wang and J. Zhu, *J. Phys. Chem. C*, 2008, **112**, 19841–19845.
44 Y. Zhou, J. Yang, T. He, H. Shi, X. Cheng and Y. Lu, *Small*, 2013, **9**, 3445–3454.
45 W. Wang, J. Cui, W. Fan, Z. Feng, X. Ma and W. Jiang, *Mater. Lett.*, 2012, **84**, 120–123.
46 L. Guardia, S. Villar-Rodil, J. Paredes, R. Rozada, A. Martínez-Alonso and J. Tascón, *Carbon*, 2012, **50**, 1014–1024.
47 S. Moussa, G. Atkinson, M. SamyEl-Shall, A. Shehata, K. M. AbouZeid and M. B. Mohamed, *J. Mater. Chem.*, 2011, **21**, 9608–9619.
48 Y.-K. Kim and D.-H. Min, *Langmuir*, 2012, **28**, 4453–4458.
49 C. Liu, K. Wang, S. Luo, Y. Tang and L. Chen, *Small*, 2011, **7**, 1203–1206.
50 C. L. Pavithra, B. V. Sarada, K. V. Rajulapati, T. N. Rao and G. Sundararajan, *Sci. Rep.*, 2014, **4**, 4049.
51 J. Yang, C. Zang, L. Sun, N. Zhao and X. Cheng, *Mater. Chem. Phys.*, 2011, **129**, 270–274.
52 Y. Qin, J. Li, Y. Kong, X. Li, Y. Tao, S. Li and Y. Wang, *Nanoscale*, 2014, **6**, 1281–1285.
53 P. Zhang, M. Fujitsuka and T. Majima, *Nanoscale*, 2017, **9**, 1520–1526.
54 Y. Y. Wang, F. Chen, X. X. Ye, T. Wu, K. B. Wu and C. Y. Li, *Sens. Actuators, B*, 2017, **245**, 205–212.
55 B. G. Rao, H. R. Matte and C. Rao, *J. Cluster Sci.*, 2012, **23**, 929–937.
56 G. Gao, A. Mathkar, E. P. Martins, D. S. Galvão, D. Gao, P. A. da Silva Autreto, C. Sun, L. Cai and P. M. Ajayan, *J. Mater. Chem. A*, 2014, **2**, 3148–3154.
57 D. Li, Y. S. Zhou, X. Huang, L. Jiang, J.-F. Silvain and Y. F. Lu, *Nanoscale*, 2015, **7**, 3651–3659.
58 Y. Shi, J.-K. Huang, L. Jin, Y.-T. Hsu, S. F. Yu, L.-J. Li and H. Y. Yang, *Sci. Rep.*, 2013, **3**, 1839.
59 E. Parzinger, B. Miller, B. Blaschke, J. A. Garrido, J. W. Ager, A. Holleitner and U. Wurstbauer, *ACS Nano*, 2015, **9**, 11302–11309.
60 A. Castellanos-Gomez, J. Quereda, H. P. van der Meulen, N. Agraït and G. Rubio-Bollinger, *Nanotechnology*, 2016, **27**, 115705.

61 T.-L. Guo, J.-G. Li, D.-H. Ping, X. Sun and Y. Sakka, *ACS Appl. Mater. Interfaces*, 2013, **6**, 236–243.
62 G. P. Lee, Y. Shi, E. Lavoie, T. Daeneke, P. Reineck, U. B. Cappel, D. M. Huang and U. Bach, *ACS Nano*, 2013, **7**, 5911–5921.
63 M. Freitag, M. Steiner, Y. Martin, V. Perebeinos, Z. Chen, J. C. Tsang and P. Avouris, *Nano Lett.*, 2009, **9**, 1883–1888.
64 S. Sahoo, A. P. Gaur, M. Ahmadi, M. J.-F. Guinel and R. S. Katiyar, *J. Phys. Chem. C*, 2013, **117**, 9042–9047.
65 C.-T. Hsieh, C. Pan and W.-Y. Chen, *J. Power Sources*, 2011, **196**, 6055–6061.
66 L. Polavarapu and Q.-H. Xu, *Langmuir*, 2008, **24**, 10608–10611.
67 C.-C. Chang, K.-H. Yang, Y.-C. Liu, T.-C. Hsu and F.-D. Mai, *ACS Appl. Mater. Interfaces*, 2012, **4**, 4700–4707.